AIAA JOURNAL
Vol. 42, No. 4, April 2004

Role of Transient Growth in Roughness-Induced Transition

Eli Reshotko*
Case Western Reserve University, Cleveland, Ohio 44106
and
Anatoli Tumin†
University of Arizona, Tucson, Arizona 85721

Surface roughness can have a profound effect on boundary-layer transition. However, the mechanisms responsible for transition with three-dimensional distributed roughness have been elusive. Various Tollmien–Schlichting-based mechanisms have been investigated in the past but have been shown not to be applicable. More recently, the applicability of transient growth theory to roughness-induced transition has been studied. A model for roughness-induced transition is developed that makes use of computational results based on the spatial transient growth theory pioneered by the present authors. For nosetip transition, the resulting transition relations reproduce the trends of the Reda and passive nosetip technology (PANT) data and account for the separate roles of roughness and surface temperature level on the transition behavior.

Nomenclature

A, B, C	=	matrices 5×5
D	=	d/dy
G	=	energy ratio parameter
k	=	height of the roughness elements
M	=	Mach number
$\boldsymbol{M}$	=	matrix in the energy norm
N	=	number of eigenmodes used in the optimization procedure
p	=	pressure
R_N	=	the nose radius
Re	=	Reynolds number
T	=	temperature
t	=	time
u	=	streamvise velocity disturbance
v	=	transverse velocity disturbance
w	=	spanwise velocity disturbance
x	=	streamwise coordinate
y	=	distance from the wall
z	=	spanwise coordinate
α	=	streamwise wave number
β	=	spanwise wave number
β_H	=	Hartree parameter
γ	=	specific heat ratio
δ	=	boundary-layer thickness
δ^*	=	displacement thickness
θ	=	momentum thickness
ν	=	kinematic viscosity
ρ	=	density
ω	=	angular frequency

Subscripts

aw	=	adiabatic wall
e	=	edge of the boundary layer
in	=	input value
s	=	mean flow parameter
tr	=	at the transition point
w	=	wall condition
θ	=	based on momentum thickness

Superscripts

T	=	transposed
$\hat{}$	=	perturbation of the parameter

Introduction

SURFACE roughness can have a profound effect on boundary-layer transition. The mechanisms associated with single roughness elements are only partially understood, whereas those responsible for transition with distributed roughness are not yet known. This has led to a large body of empirical information in the literature that is not fully consistent. These dimensionless correlations are generally based on two-dimensional parameters such as Reynolds number Re_k, k/δ^*, or k/δ, whereas distributed roughness is inherently three dimensional. The three dimensionality is usually introduced by providing separate curves in the correlations for each three-dimensional shape and distribution. Nevertheless, these correlations are still the operative database for incorporating the effects of distributed roughness in design. Because the fundamental mechanisms are not known, there is considerable uncertainty in the reliability and extrapolability of such correlations.

The first author is one of a number of investigators who in the past have pursued a Tollmien–Schlichting (T–S) explanation for the effects of roughness, both discrete and distributed. Only discrete two-dimensional roughness elements yield to a T–S explanation.[1] The attempts to find a T–S explanation for three-dimensional roughness, both discrete and distributed, have failed. These attempts have been documented by Reshotko[2] and Morkovin.[3]

Experimental studies by Reshotko and Leventhal,[4] Corke et al.,[5] and Tadjfar et al.[6] have presented some of the physical observations of flow over distributed roughness. It is generally agreed that roughness displaces the mean flow outward, affecting the profiles only within the roughness height. Subcritical amplification is observed principally at low frequencies, and the growth can easily reach nonlinear levels quickly. It is suspected that, in common with single three-dimensional roughness elements, the distributed roughness gives rise to vortex structures emanating from the elements. These vortices are primarily streamwise. Reshotko[2] and Morkovin[3,7] have summarized these observations.

A possible unifying explanation for these observations lies in the mechanism of transient growth. Transient growth arises through the

Presented as Paper 2002-2850 at the AIAA 32nd Fluid Dynamics Conference, St. Louis, MO, 24–27 June 2002; received 20 September 2002; revision received 22 March 2003; accepted for publication 1 July 2003.

*Kent H. Smith Professor Emeritus of Engineering, Department of Mechanical and Aerospace Engineering. Fellow AIAA.

†Associate Professor, Department of Aerospace and Mechanical Engineering. Senior Member AIAA.

coupling between slightly damped, highly oblique (nearly streamwise), Orr–Sommerfeld and Squire modes leading to algebraic growth followed by exponential decay outside the T–S neutral curve. A weak transient growth can also occur for two-dimensional or axisymmetric modes because the Orr–Sommerfeld operator (also its compressible counterpart) is not self-adjoint; therefore, its eigenfunctions are not strictly orthogonal.

In recent papers, the authors have shown the potential importance of transient growth in explaining the long standing blunt-body paradox[8] and have completed papers on the role of transient growth in Poiseuille pipe flow[9] and boundary-layer flow.[10] These three papers are the first to use a spatial growth formulation of these transient growth problems rather than the earlier temporal growth approach.

Because transient growth factors can be extremely large in flows that are T–S stable or in parameter ranges that are T–S stable, transient growth is an attractive mechanism to consider with respect to distributed roughness effects. Recent works by Luchini[11] and by Tumin and Reshotko[10] show that, for Blasius flow, maximum transient growth factors are for streamwise (stationary, zero-frequency) disturbances. As the frequency increases, the growth factors are reduced.

Spatial Theory of Optimal Disturbances

The spatial formulation of the transient growth theory within the scope of linearized Navier–Stokes equations was introduced in Refs. 8–10. For the sake of consistency, we recapitulate briefly the key elements of the theoretical model.

The linearized Navier–Stokes equations for three-dimensional disturbances $\sim \exp[i(\alpha x + \beta z - \omega t)]$ of prescribed frequency ω and transverse wave number β are reduced to a system of ordinary differential equations in the following form:

$$(AD^2 + BD + C)\Phi = 0 \tag{1}$$

where $\Phi = [\hat{u}(y), \hat{v}(y), \hat{p}(y), \hat{T}(y), \hat{w}(y)]^T$ is a five-element vector comprising the complex amplitude functions for the x and y components of velocity, pressure, and temperature and z component of velocity where superscript T stands for the vector transpose. A, B, and C are 5×5 matrices. (Nonzero elements are given in the Appendix of Ref. 10.) The boundary conditions for Eq. (1) are

$$\begin{aligned} y = 0: &\qquad \Phi_1 = \Phi_2 = \Phi_4 = \Phi_5 = 0 \\ y \to \infty: &\qquad |\Phi_j| < \infty \end{aligned} \tag{2}$$

Boundary condition (2) outside the boundary layer allows decaying eigenmodes ($y \to \infty : \Phi_1, \Phi_2, \Phi_4, \Phi_5 \to 0$) that represent the discrete spectrum and nongrowing, nondecaying modes, as well, that represent the continuous spectrum.

The signaling problem suggests that at the moment of time $t = 0$ a localized disturbance source is switched on. Analysis of the linearized Navier–Stokes equations under the assumption that the downstream and upstream boundaries are at $\pm\infty$ leads to the conclusion that only branches corresponding to the decaying modes of the continuous spectrum apply to the solution downstream of the source.

Following from the signaling problem, the flowfield downstream of a disturbance source may be represented as an expansion in eigenfunctions including the decaying modes of the continuous and discrete spectrum plus any growing discrete modes if present. Having selected the downstream eigenmodes, one can continue the analysis as an initial value problem spanned by the eigenmodes, and the method of analysis developed by Schmid and Henningson[12] for temporal stability theory may be applied.

We introduce a vector–function $\boldsymbol{q} = (\hat{u}, \hat{v}, \hat{\rho}, \hat{T}, \hat{w})^T$ and a scalar product

$$(\boldsymbol{q}_1, \boldsymbol{q}_2)_2 = \int_0^\infty \boldsymbol{q}_1^H \boldsymbol{M} \boldsymbol{q}_2 \, dy \tag{3}$$

where the matrix $\boldsymbol{M}$ is

$$\boldsymbol{M} = \mathrm{diag}\left\{\rho_s, \rho_s, T_s \Big/ \left(\gamma \rho_s M_e^2\right), \rho_s \Big/ \left[\gamma(\gamma - 1) T_s M_e^2\right], \rho_s\right\} \tag{4}$$

The definition of the scalar product (3) leads to the energy norm introduced by Mack[13]:

$$\|\boldsymbol{q}\|^2 = (\boldsymbol{q}, \boldsymbol{q})_2 = \int_0^\infty \boldsymbol{q}^H \boldsymbol{M} \boldsymbol{q} \, dy \tag{5}$$

Expanding the vector–function $\boldsymbol{q}$ into N decaying eigenmodes (which might belong to the discrete spectrum or to the numerical discretization of the continuous spectrum), we obtain

$$\boldsymbol{q}(t, x, y, z) = e^{i(\beta z - \omega t)} \sum_{k=1}^{N} \kappa_k \hat{\boldsymbol{q}}_k(y) e^{i\alpha_k x} \tag{6}$$

The vector–function $\hat{\boldsymbol{q}}_k = (\hat{u}_k, \hat{v}_k, \hat{\rho}_k, \hat{T}_k, \hat{w}_k)^T$ comprises three velocity components, density, and temperature perturbations corresponding to kth eigenfunction. The coefficients κ_k are optimized to achieve the maximum energy growth at the specific downstream coordinate:

$$G(\beta, \omega, Re, x) = \max\left(\|\boldsymbol{q}(x)\|^2 \Big/ \|\boldsymbol{q}_0\|^2\right) \tag{7}$$

where $\|\boldsymbol{q}_0\|^2$ corresponds to the energy at the initial location.

One may find details of the numerical procedure for the base flow and for the eigenmode analysis in Ref. 10. To consider the curvature effect, the governing equations were written in spherical coordinates under the parallel flow approximation. The latter led to the appearance of the ratio y/R_N in the coefficients and some new terms, that is, centrifugal terms. The curvature-associated corrections of the coefficients were neglected in the viscous terms of the equations.

Although the numerical results in Ref. 10 (and in the present work) were obtained under the parallel flow approximation, recent nonparallel results[14] within the scope of partial differential equations demonstrate that the approximation is satisfactory for the quantitative and qualitative analysis of the transient growth phenomena.

Transient Growth Calculations

A. Zero Pressure Gradient (Flat Plates or Cones)

Spatial transient growth calculations have been performed for zero pressure gradient boundary layers (Hartree parameter $\beta_H = 0$) at Mach numbers from 1.5 to 6 and for a range of surface temperatures $0.25 < T_w/T_{aw} < 1.0$. The calculations are all for stationary disturbances, $\omega = 0$. These results are summarized in Fig. 1. Consistent with expectations from the transient growth theory, the growth factors scale with length Reynolds number or the square of a thickness Reynolds number. For $0.75 < T_w/T_{aw} < 1.0$, the growth factors

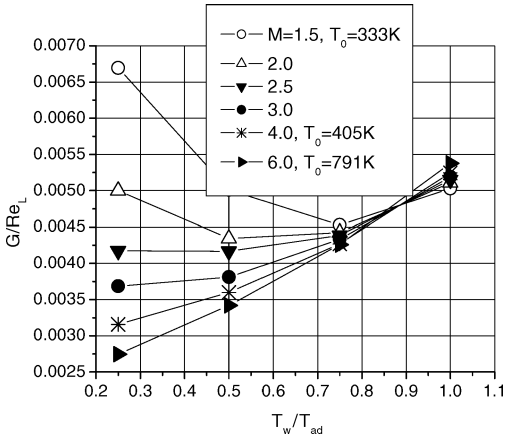

Fig. 1 Optimal growth factors for zero pressure gradient; $Re_L = 9 \times 10^4$.

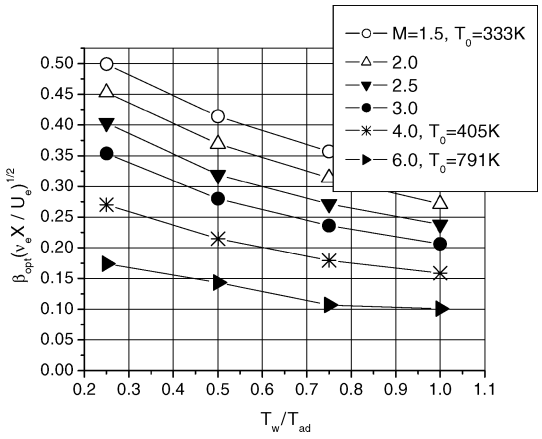

Fig. 2 Optimal spanwise wavenumber for zero pressure gradient; $Re_L = 9 \times 10^4$.

are essentially independent of Mach number, whereas for colder walls, the lower the Mach number is, the higher the growth rate. The corresponding optimal spanwise wave numbers are shown in Fig. 2. For all cases, the optimal spanwise wavelengths are from 3 to 3.5 boundary-layer thicknesses. For the cold wall case ($T_w/T_{\text{aw}} = 0.25$), the optimal transient growth factors are very sensitive to Mach number and can be summarized by the following relation:

$$G^{\frac{1}{2}}/Re_\theta = 0.0619 + 0.0905/M_e \tag{8}$$

This relation can be later used to estimate the effect of roughness on transition for flat plates or cones.

B. Stagnation Point Flow

Extensive calculations have also been carried out for axisymmetric stagnation point flows, $\beta_H = 0.5$. These are relevant to the hypersonic sphere–cone nosetip configurations for which there is an extensive experimental database and significant transition correlations.[15–18] The calculations were first performed for $T_w/T_{\text{aw}} = 0.25$. However, because most of the experimental database is centered around $T_w/T_{\text{aw}} = 0.5$, the results for the latter case will be emphasized here. Furthermore, in contrast to the flat plate, curvature is a significant factor for the sphere. Curvature is included in our calculations and in the results to be presented.

For surface temperatures in the vicinity of $T_w/T_{\text{aw}} = 0.5$, the transient growth results without curvature effects are shown in Fig. 3. The optimal spanwise wave number is essentially constant over the Mach number range at $\beta_{\text{opt}}\theta = 0.28$, which corresponds to about 3.2 boundary-layer thicknesses. The curvature effects were included into the following correlations through the ratio G/G_0 of the energy growth factors with and without the curvature associated terms. At a prescribed temperature level, the result might depend on the radius of curvature, the Reynolds number, and the local Mach number. For each combination of parameters, the optimization procedure has to be carried out with respect to the spanwise wave number, and the computations become very time-consuming. Initially, we computed the effect of local Mach number on the ratio at a prescribed Reynolds number $Re_\theta = 123$. Because the results did not reveal any significant effect of the Mach number, simultaneous effects of curvature and the local Reynolds number were investigated at $M_e = 0.8$. In these evaluations, three Reynolds numbers, $Re_\theta = 82$, 123, and 410, were chosen for consideration at different curvature parameters, θ/R_N. Figure 4 shows the simultaneous effect of the Reynolds number and the curvature parameter on the ratio $(G/G_0)^{1/2}$ The larger the curvature is (smaller nose radius), the smaller the growth factor. This stabilizing effect agrees with previous experimental observations.[16] Figure 4 also shows a suggested curve fit for these data. Because most of the experimental runs had surface temperature level variations during the run, and because the growth factors are sensitive to surface temperature level, it has further been determined from a least-squares fit of the peak values in Fig. 3 of Ref. 8 that $G^{1/2}$

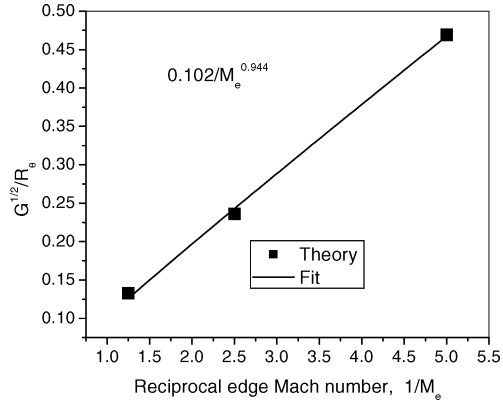

Fig. 3 Optimal growth factors for axisymmetric stagnation point flow; $T_w/T_{\text{aw}} = 0.5$.

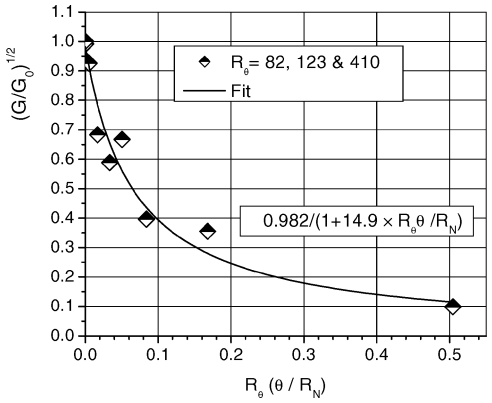

Fig. 4 Effect of curvature on optimal growth factor for axisymmetric stagnation point flow $M_e = 0.8$ and $T_w/T_{\text{aw}} = 0.5$.

varies as $(T_w/T_{\text{aw}})^{-0.77}$ in the vicinity of $T_w/T_{\text{aw}} = 0.5$. This can be summarized by

$$G^{\frac{1}{2}} = \frac{0.1\left(Re_\theta / M_e^{0.944}\right)(2T_w/T_{\text{aw}})^{-0.77}}{1 + 14.9Re_\theta(\theta/R_N)} \tag{9}$$

Influence of Roughness on Transition

The influence of roughness on transition can be modeled in a manner similar to that used by Andersson et al.[19] for freestream turbulence effects on transition. We assume that an energy norm at transition is related to an input energy through the transient growth factor G:

$$E_{\text{tr}} = GE_{\text{in}} \tag{10}$$

The input energy is in the form of a density times velocity squared where the roughness-induced disturbance velocities are assumed proportional to the roughness height k. The momentum thickness θ is chosen as the reference length because it is the least sensitive to surface temperature level of any of the boundary-layer scales. For stagnation point flow, θ is also constant with distance from the stagnation point. The resulting expression for E_{in} is

$$E_{\text{in}} = (\rho_w/\rho_e)(k/\theta)^2 \tag{11}$$

For a boundary layer, Eq. (11) can be approximated:

$$E_{\text{in}} = (T_e/T_w)(k/\theta)^2 \tag{12}$$

Again, the growth factor G scales with the square of a thickness Reynolds number or with length Reynolds number to the one power. Thus, from Eqs. (10) and (12), we can write

$$(E_{\text{tr}})^{\frac{1}{2}} = \left(G^{\frac{1}{2}}/Re_\theta\right)Re_\theta(k/\theta)(T_e/T_w)^{\frac{1}{2}} \tag{13}$$

where $G^{1/2}/Re_\theta$ is obtained from the transient growth results for the particular geometry and flow parameters. Transition is assumed to occur when, for the given flow, E_{tr} reaches a specific value, here taken as a constant.

A. Zero Pressure Gradient (Flat Plates or Cones)

With the result of Eq. (8) used in Eq. (13), the transition relation for zero pressure gradient flows with $T_w/T_{aw} = 0.25$ would be

$$(0.0619 + 0.0905/M_e) \times Re_{\theta,tr}(k/\theta)(T_e/T_w)^{\frac{1}{2}} = \text{const} \qquad (14)$$

The latter leads to the roughness-induced transition criterion

$$Re_{\theta,tr} \sim (k/\theta)^{-1}(T_e/T_w)^{-\frac{1}{2}} \qquad (14a)$$

B. Stagnation Point Flow

According to Eq. (13), we have to extract the factor $G^{1/2}/Re_\theta$ from the transient growth results. The calculations summarized by Eq. (9) are for parallel flows ($M_e = \text{const}$). However, for the stagnation point flow, the edge Mach number varies almost linearly with angle from the stagnation point. From Eq. (9), it is seen that

$$G^{\frac{1}{2}}/Re_\theta \sim 1/M_e^{0.944} \qquad (15)$$

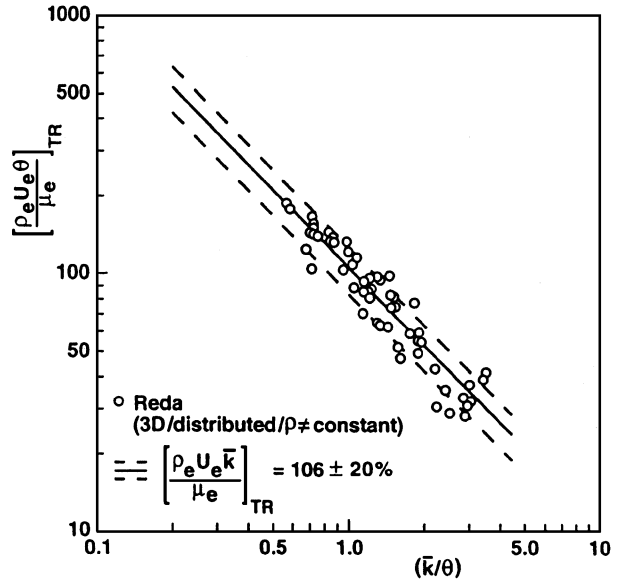

Fig. 5 Nosetip transition data from ballistic-range experiments; three-dimensional distributed roughness.[17,18]

Thus, the growth factor is largest near the stagnation point and diminishes rapidly as the edge Mach number increases. An integration of the differential growth factors from the stagnation point to any downstream location shows that the integrated growth factor is essentially constant beyond $M_e \sim 0.1$, and therefore, $G^{1/2}/Re_{\theta,tr}$ is essentially independent of the local Mach number at the transition location.

Thus, for the stagnation point in the vicinity of $T_w/T_{aw} = 0.5$, the relation is

$$\frac{Re_{\theta,tr}(k/\theta)(T_e/T_w)^{\frac{1}{2}}(2T_w/T_e)^{-0.77}}{[1 + 14.9Re_\theta(\theta/R_N)]} = \text{const} \qquad (16)$$

The last relation shows the trends of transition Reynolds number with roughness height and surface temperature level. For constant surface temperature level, Reynolds number $Re_{\theta,tr}$ should vary as $(k/\theta)^{-1}$. This is consistent with Reda's ballistic range data[17,18] as shown in Fig. 5.

The passive nosetip technology (PANT) wind-tunnel data[15,16] shown in Figs. 6a and 7a display this trend as well. In addition, some of the PANT data were taken for nearly constant (k/θ), but with varying surface temperature about $T_w/T_{aw} = 0.5$. For this case, Eq. (16) shows that $Re_{\theta,tr}$ should vary as $(T_w/T_e)^{1.27}$. This again is supported by the PANT data, as shown by comparison of the data with lines of slope $n = 1.27$ in Figs. 6b and 7b. Note that all of the nosetip transitions in the PANT database take place well within the sonic point on the sphere ($0.2 < M_{e,tr} < 0.8$) and with $20 < Re_{\theta,tr} < 120$.

In treating these data, only the "revised data" are used here. The revised data are based on the Batt and Legner[15,16] protocol of identifying transition location. The roughness heights are those of the original PANT data.[20,21] The present summary relation for the PANT database is

$$Re_{\theta,tr} = 180(k/\theta)^{-1}(T_e/2T_w)^{-1.27} \qquad (17)$$

The curvature factor is ignored because it varies only within a narrow range for the whole database. The numerical factor of 180 is for $T_w/T_{aw} = 0.5$ and comes from averaging in only those points for which $0.45 < T_w/T_{aw} < 0.55$. The broken lines on either side of the solid line in Figs. 6a and 7a show the expected data spread for $0.45 < T_w/T_e < 0.55$ according to Eq. (17).

Whereas the Reda correlation (Fig. 5)[17,18] and the present correlation of the PANT data [Eq. (17)] both vary as $(k/\theta)^{-1}$ for constant surface temperature, Reda's ballistic range data and the PANT wind-tunnel data were taken at different temperature levels. Because θ appears in the numerator of both sides of Eq. (17), this relation can be rewritten as

$$U_e k/\nu_e = 180(2T_w/T_e)^{1.27} \qquad (18)$$

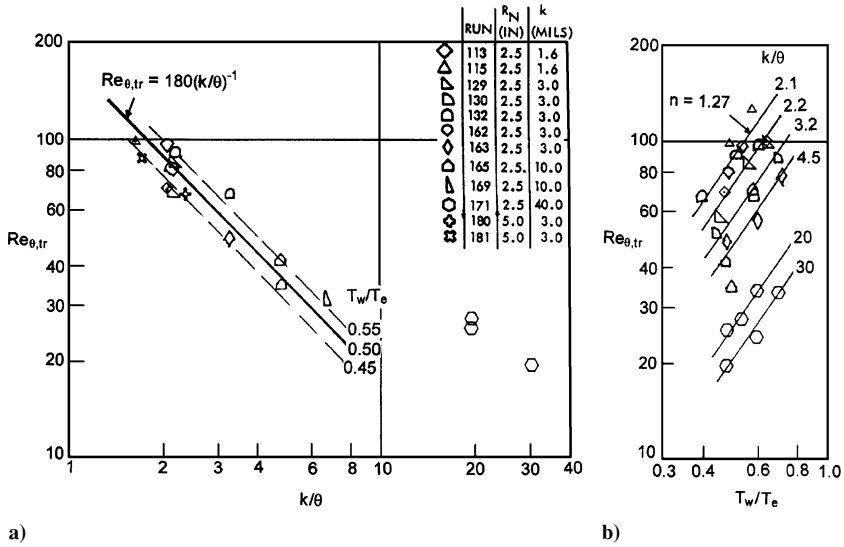

Fig. 6 Transient-growth-based transition correlations of PANT series A data.

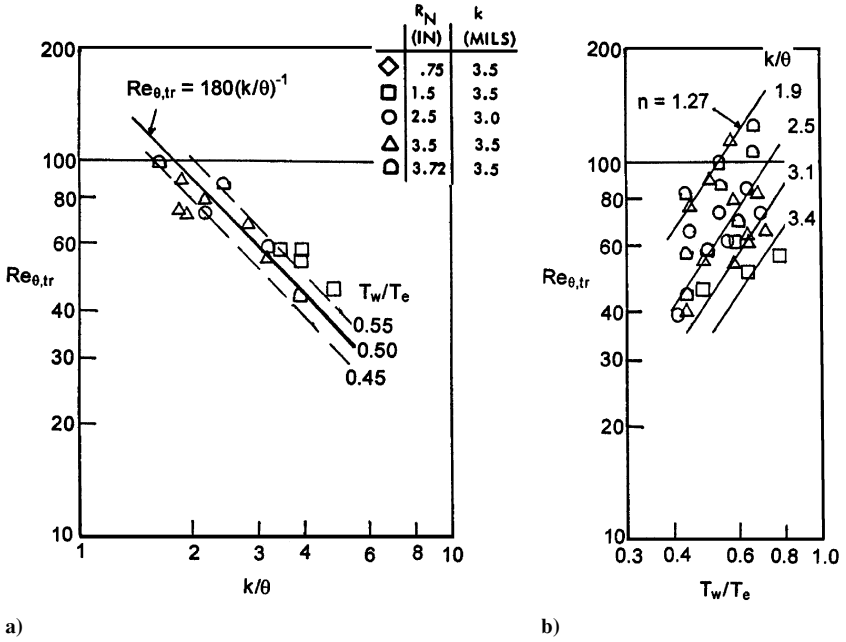

Fig. 7 Transient growth based transition correlations of PANT series J data.

The left-hand side of Eq. (18) is the same as Reda's[17,18] Reynolds number $Re_{ke,\mathrm{tr}}$. For $T_w/T_{\mathrm{aw}} = 0.33$, Eq. (18) gives Reda's value of 106 (Fig. 5). Reda in a private communication in 2002 estimates his surface temperature level to have been about 0.3. Thus, the two data sets are also quantitatively comparable.

Summary

Under parallel flow assumptions, transient growth calculations have been performed for zero pressure gradient and stagnation point flows over Mach number and surface temperature ranges that are relevant to slender and blunt hypersonic configurations. In addition, a model for roughness-induced transition has been developed that makes use of the transient growth results.

For nosetip transition, the dominant transient growth takes place in the near vicinity of the stagnation point so that the resulting correlation is independent of the local Mach number at the transition location. This yields transition relations that reproduce the trends of the Reda and PANT data but with exponents for roughness and surface temperature effects obtained from the transition modeling and the transient growth theory.

The authors, therefore, believe that transient growth is a very promising explanation for early transition due to distributed roughness.

Acknowledgments

This work is supported by the U.S. Air Force Office of Scientific Research. The first author thanks Daniel C. Reda for fruitful discussions regarding roughness characterization and correlating roughness Reynolds numbers.

References

[1]Klebanoff, P. S., and Tidstrom, K. D., "Mechanism by Which a Two-Dimensional Roughness Element Induces Boundary-Layer Transition," *Physics of Fluids*, Vol. 15, 1972, pp. 1173–1188.

[2]Reshotko, E., "Disturbances in a Laminar Boundary Layer Due to Distributed Surface Roughness," *Turbulence and Chaotic Phenomena in Fluids*, edited by T. Tatsumi, Elsevier, New York, 1984, pp. 39–46.

[3]Morkovin, M. V., "Panel Summary on Roughness," *Instability and Transition*, edited by M. Y. Hussaini and R. G. Voight, Vol. 1, Springer-Verlag, Berlin, 1990, pp. 265–271.

[4]Reshotko, E., and Leventhal, L., "Preliminary Experimental Study of Disturbances in a Laminar Boundary-Layer Due to Distributed Surface Roughness," AIAA Paper 81-1224, June 1981.

[5]Corke, T. C., Bar-Sever, A., and Morkovin, M. V., "Experiments on Transition Enhancement by Distributed Roughness," *Physics of Fluids*, Vol. 29, 1986, pp. 3199–3213.

[6]Tadjfar, M., Reshotko, E., Dybbs, A., and Edwards, R. V., "Velocity Measurements Within Boundary Layer Roughness Elements Using Index Matching," *International Symposium on Laser Anemometry*, edited by A. Dybbs and E. Pfund, FED Vol. 33, American Society of Mechanical Engineers, Fairfield, NJ, 1985, pp. 59–73.

[7]Morkovin, M. V., "On Roughness-Induced Transition: Facts, Views & Speculation," *Instability and Transition*, edited by M. Y. Hussaini and R. G. Voight, Vol. 1, Springer-Verlag, Berlin, 1990, pp. 281–295.

[8]Reshotko, E., and Tumin, A., "The Blunt Body Paradox—A Case for Transient Growth," *Laminar–Turbulent Transition*, edited by H. F. Fasel and W. S. Saric, Springer, New York, 2000, pp. 403–408.

[9]Reshotko, E., and Tumin, A., "Spatial Theory of Optimal Disturbances in a Circular Pipe Flow," *Physics of Fluids*, Vol. 13, 2001, pp. 991–996.

[10]Tumin, A., and Reshotko, E., "Spatial Theory of Optimal Disturbances in Boundary Layers," *Physics of Fluids*, Vol. 13, 2001, pp. 2097–2104.

[11]Luchini, P., "Reynolds-Number-Independent Instability of the Boundary Layer over a Flat Surface: Optimal Perturbations," *Journal of Fluid Mechanics*, Vol. 404, 2000, pp. 289–309.

[12]Schmid, P. J., and Henningson, D. S., "Optimal Energy Density Growth in Hagen–Poiseuille Flow," *Journal of Fluid Mechanics*, Vol. 277, 1994, pp. 197–225.

[13]Mack, L. M., "Boundary Layer Stability Theory," Jet Propulsion Lab., JPL Rept. 900-277, California Inst. of Technology, Pasadena, CA, Nov. 1969.

[14]Tumin, A., and Reshotko, E., "Optimal Disturbances in Compressible Boundary Layers," *AIAA Journal*, Vol. 41, No. 12, 2003, pp. 2357–2363.

[15]Batt, R. G., and Legner, H. L., "A Review and Evaluation of Ground Test Data on Roughness Induced Nosetip Transition," Ballistic Missile Office/SYDT, Rept. BMD-TR-81-58, Norton AFB, CA, Oct. 1980.

[16]Batt, R. G., and Legner, H. L., "A Review of Roughness-Induced Nosetip Transition," *AIAA Journal*, Vol. 21, No. 1, 1983, pp. 7–22.

[17]Reda, D. C., "Correlation of Nosetip Boundary-Layer Transition Data Measured in Ballistic Range Experiments," *AIAA Journal*, Vol. 19, No. 3, 1981, pp. 329–339.

[18]Reda, D. C., "Review and Synthesis of Roughness-Dominated Transition Correlations for Reentry Applications," *Journal of Spacecraft and Rockets*, Vol. 39, No. 2, 2002, pp. 161–167.

[19]Andersson, P., Berggren, M., and Henningson, D., "Optimal Disturbances and Bypass Transition in Boundary Layers," *Physics of Fluids*, Vol. 11, 1999, pp. 135–150.

[20]Jackson, M. D., and Baker, D. L., "Interim Report Passive Nosetip Technology (PANT) Program," *Surface Roughness Effects, Part I. Experimental Data*, U.S. Air Force Space and Missile Systems Organization, SAMSO-TR-74-86, Vol. 3, Los Angeles, Jan. 1974.

[21]Anderson, A. D., "Interim Report Passive Nosetip Technology (PANT) Program," *Surface Roughness Effects, Part III, Boundary Layer Transition Correlation and Analysis*, U.S. Air Force Space and Missile Systems Organization, SAMSO-TR-74-86, Vol. 3, Los Angeles, Jan. 1974.

W. J. Dahm
Associate Editor